Steady state model of the AC/DC convertor in the harmonic domain

B.C. Smith
N.R. Watson
A.R. Wood
J. Arrillaga

Indexing terms: HVdc, Convertors, Harmonics

Abstract: A set of equations are developed that describe the 6-pulse convertor in the steady-state harmonic domain. The method used is to directly convolve in the harmonic domain the DC voltage in each conduction period, with an appropriate sampling function. This avoids the need to use transfer functions, FFTs, or complicated Fourier transforms. The technique is fast and simple, and is able to model effects that have, until now, been largely ignored (such as the DC-ripple effect on commutation duration). Moreover, the equations are suitable for inclusion in a Newton-type solution method, as the partial derivatives are easily obtained.

List of symbols

$\otimes$ = convolution operator
Re = real part of
Im = imaginary part of
D = commutating current DC offset
E_d = constant DC-voltage source
F_{I_k} = order k DC-current mismatch
F_{θ_i} = firing i mismatch
$F_{\phi i}$ = commutation mismatch
G = current transducer gain
I_a = phase-A current into convertor
I_c = commutating current
I_{d0} = average DC current or current order
I_d = DC side current (sum of phasors)
L_x = commutating reactance in phase x
$L_{eb} = L_e + L_b$
n_h = number of harmonics to be analysed
P = current controller proportional gain
T = current transducer time constant
T_I = current controller integrator time constant
V_{d0} = average DC voltage
V_d = DC voltage (sum of phasors)
V_{dp} = DC voltage, sample p (sum of phasors)
V_{eb} = commutating voltage (sum of phasors)
V_t = terminal voltage for ideal convertor
X_c = commutating reactance for ideal convertor
Y_{d0} = DC-system admittance

Paper 1729C (P6, P7), first received 3rd May and in revised form 14th November 1994

The authors are with the Department of Electrical and Electronic Engineering, University of Canterbury, Christchurch, New Zealand

α = instantaneous alpha order (sum of phasors)
β_i = timing reference for ith firing
θ_i = ith firing angle
ϕ_i = ith end of commutation angle
Ψ_p = the pth sampling function (sum of phasors)
ω = AC side fundamental frequency

Subscripts

e = phase commutating off
b = phase commutating on
o = the remaining phase
(during commutation)
i = commutation or firing number
$+$ = phase connected to positive DC rail
$-$ = phase connected to negative DC rail
(not commutating)
p = sample number
k = kth harmonic component

1 Introduction

The main motivation for the modelling of AC/DC convertors in the harmonic domain is computational efficiency, since time-domain simulations must run until transients have decayed. However, there are several challenging interactions that must be included in a comprehensive harmonic-domain convertor model, and to date no model accommodates them all.

The following are important considerations that must be taken into account in a complete harmonic model of the convertor:

1. The convertor terminal voltage may be unbalanced and include harmonic components.
2. There is a voltage drop across the commutating impedance, due to phase-current harmonics.
3. The commutating impedances may be unbalanced.
4. There is a conducting voltage drop across the valves.
5. The firing instants are a function of the controller and periodic convertor variables (for example the DC ripple and terminal voltage harmonics).
6. The commutation current is affected by the AC voltage and DC-current harmonics.
7. Each commutation ends when the instantaneous commutation current is equal to the instantaneous DC current. The DC ripple therefore affects the overlap angles.
8. The DC voltage is a function of the unbalanced and

distorted AC voltages, the irregular firing and overlap angles, and the voltage drop across the commutating impedance.

9. The AC-phase currents are a function of the irregular (i.e. not spaced by 60 degrees) firing and overlap angles, the commutation currents, and also of the DC-current harmonics.

Yacamini and de Oliveira [1], in 1980, developed a harmonic convertor model that included most of the above items. However, in the calculation of the overlap angle, the effect of DC harmonics (items 6 and 7) was not included. This has subsequently been shown by Wood [2] to have a significant effect on the convertor harmonic response. In 1986, Yacamini and Oliveira [3] extended the previous work, by modelling the firing angle variation over a cycle, and including aspects of the DC ripple. The Fourier coefficients of the phase currents were obtained by a direct analytic Fourier integral of the commutation and DC currents. The method used to calculate the overlap angle from the commutation current was not specified.

A convertor model was also developed for the iterative harmonic analysis (IHA) program by Eggleston [4]. This model, although developed for harmonic studies, nevertheless makes regular excursions into the time domain, to build up the phase currents point by point. An FFT is performed on the sampled waveforms to obtain the harmonic components of the phase currents. When embedded in a Gauss–Seidel solution, the IHA model has displayed convergence problems. Callaghan [5] related the convergence problems to triplen harmonic magnification between iterations, and to the AC system reactance. Callaghan investigated several techniques for overcoming these problems. Recently, elaborate convergence aids have been described by Carbone *et al.* [6]. A matched impedance pair is inserted between the convertor and AC system to modify the convergence properties of the system, without changing the system electrically.

A better method of solving nonlinear systems is to use Newton's method, where the system is linearised at each iteration. A convertor model suitable for this method has been developed by Valcárcel [7], which assumes no DC ripple. A shortcoming of this model is that all the firing and overlap angles are not related to the other system variables in the Jacobian matrix, although there is certainly some dependence. Because of the above points, we expect impaired convergence and accuracy in more difficult systems, especially for high-order harmonics.

A comprehensive convertor model has been described by Ferreira [8], which includes all the points listed above apart from item 3. However, the generality of this model is restricted by the use of a poor solution technique, and results are only obtained efficiently on the assumption of a ripple-free DC current.

The recent model by Wood [2] represents a general linearised solution of the convertor for small levels of distortion. This model uses a transfer function approach, where the transfer functions, by means of modulation theory, have been expressed in terms of switching instants, that are themselves modulated as a result of applied distortions. The modulation of the switching instants, and the transfer function shapes, involve approximations valid only for small levels of distortion, and low-order harmonics. However, since the model is analytic, it has resulted in a better understanding of the convertor nonlinearity. As a result of employing a linearised modulation analysis, the model is valid for any frequency of applied distortion, not just harmonics.

A general set of non-linear equations is derived in this paper to describe harmonic transfer through the AC/DC convertor in the steady state. The goal of the model is to achieve an accurate solution of the convertor for all harmonics up to the 50th, by means of an iterative procedure that is also robust and fast. Unlike previous methods, which must Fourier transform time-domain quantities, the proposed formulation convolves periodic sampled quantities in the harmonic domain with their sampling functions, so that no Fourier transform is required, resulting in substantial computational savings. The sampling functions are defined in terms of the exact switching instants, which are obtained by an iterative procedure that accurately models the effect of AC voltage and DC-current distortion on the conduction periods. At present, the model takes one cycle of the AC voltage as the fundamental, and so only harmonics are analysed. In the future, an extension to the steady state over several cycles would allow inter-harmonics to be solved.

2 Derivation of the convertor equations

Analysis of the convertor in the steady state is undertaken by observing that, in each cycle, the convertor passes through a sequence of twelve internal states; these internal states being described by the conduction pattern of the valves making up the Graetz bridge. During each state, the convertor can be represented by a passive linear circuit, and if there is no energy loss in the convertor during each state, the representative linear circuits can be analysed by means of complex harmonic phasors. This is because at each state transition, the convertor enters a new steady state corresponding to the new equivalent circuit.

If the convertor is operating normally, then the conduction pattern for each state is known, and the overall state of the convertor is specified by the angles of the state transitions. These angles are the switching instants corresponding to the six firing angles, and the six end of commutation angles. The firing instants are obtained from an analysis of the convertor controller, while the ends of commutations are derived from the commutation circuits.

Once the convertor switching instants are known, the convertor response to an applied terminal voltage is characterised by means of a Fourier analysis in the harmonic domain. The DC voltage is obtained by solving each of the twelve linear circuits for the DC voltage. The overall DC voltage is obtained by convolving the twelve voltage samples with sampling functions that have a value of one during the appropriate state, and a value of zero during all other states. The Euler coefficients of the sampling functions are themselves functions of the switching instants. Cross-coupling between harmonics is therefore calculated by convolution in this model; the cross coupling being determined by the switching instants. The phase currents are obtained in a similar manner using the same sampling functions.

The steady-state equations developed here are expressed in terms of complex harmonic phasors. This means that efficient complex algebra can be used when the equations are coded in FORTRAN, and affords compatibility with other harmonic analysis programs.

2.1 Commutation analysis

The commutation circuit to be analysed is that of Fig. 1, where V_e, V_b, I_c and I_d are sums of harmonic phasors.

Although the commutating resistance is significant, it is to be included in the AC system when a full solution is undertaken, and not in the convertor model. Accounting for the commutating resistance in the commutation

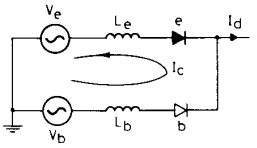

Fig. 1 *Circuit for commutation analysis*
e = ending conduction
b = beginning conduction

analysis leads to complicated, non-phasor type solutions for the commutating current [1, 8]. This must be avoided since a phasor solution for the commutating current is required in the convolution method. In this diagram valve 'e' is commutating off, whilst valve 'b' is commutating on. The commutation ends when $I_c = I_d$.

Summing voltage drops around the commutating current loop

$$V_{eb} + L_{eb}\frac{dI_c}{dt} - L_e\frac{dI_d}{dt} = 0 \tag{1}$$

or

$$\frac{dI_c}{dt} = \frac{L_e}{L_{eb}}\frac{dI_d}{dt} - \frac{V_{eb}}{L_{eb}} \tag{2}$$

Eqn. 2 can be rewritten in terms of phasors

$$I_{c_k} = \frac{jk\omega L_e I_{d_k} - V_{eb_k}}{jk\omega L_{eb}} \tag{3}$$

for the k-th harmonic phasor component, and

$$I_c(t) = D + \text{Im}\left\{\sum_{k=1}^{n_h} I_{c_k} e^{jk\omega t}\right\} \tag{4}$$

where

$$D = -\text{Im}\left\{\sum_{k=1}^{n_h} I_{c_k} e^{jk\theta_i}\right\} \tag{5}$$

D ensures that the steady state commutation current is zero at the instant of firing. For incorporation into Newton's method, eqn. 4 is written as a steady-state mismatch equation. The mismatch is the current in the valve that is commutating off, which at the end of the commutation should be zero. This is obtained by substituting $\omega t = \phi_i$ into eqn. 4.

$$F_{\phi_i} = \text{Im}\left\{j(D - I_{d_0}) + \sum_{k=1}^{n_h} F_{\phi_{i_k}} e^{jk\phi_i}\right\} = 0 \tag{6}$$

where $F_{\phi_{i_k}} = I_{d_k} - I_{c_k}$, eqn. 6 is the real valued commutation mismatch equation. When the only unknown in this equation is ϕ_i, three iterations of the single variable Newton–Raphson technique give a mismatch of less than 10^{-6} p.u. The partial derivatives of eqn. 6 are readily obtained; for the single variable case

$$\frac{\partial F_{\phi_i}}{\partial \phi_i} = \text{Im}\left\{\sum_{k=1}^{n_h} jkF_{\phi_{i_k}} e^{jk\phi_i}\right\} \tag{7}$$

2.2 Calculation of the firing instants

A firing instant occurs when the elapsed angle from a timing pulse is equal to the instantaneous value of the alpha order. The alpha order is a command variable from the convertor controller. The controller modelled here is a constant current control of the proportional integral type (Fig. 2).

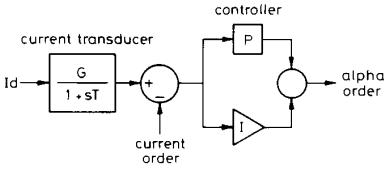

Fig. 2 *Current controller*

From Fig. 2, the alpha order can be expressed as a sum of harmonic phasors

$$\alpha = \text{Im}\left\{j\alpha_0 + \sum_{k=1}^{n_h} \alpha_k e^{jk\omega t}\right\} \tag{8}$$

where

$$\alpha_k = \frac{G}{1 + jk\omega T}\left(P + \frac{1}{jk\omega T_I}\right) I_{d_k} \tag{9}$$

With reference to Fig. 3, it can be seen that firing occurs when the elapsed angle from the equidistant timing reference is equal to the instantaneous value of the alpha order, i.e. $\alpha = \theta_i - \beta_i$. The firing mismatch equation is therefore

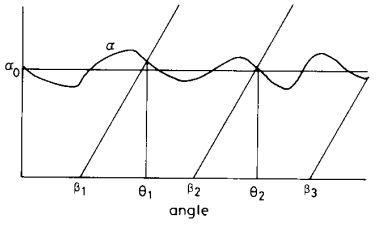

Fig. 3 *Method of finding the firing instants: the timing instants are assumed perfectly equidistant (π/3)*

$$F_{\theta_i} = \text{Im}\left\{j(\beta_i + \alpha_0 - \theta_i) + \sum_{k=1}^{n_h} \alpha_{i_k} e^{jk\theta_i}\right\} = 0 \tag{10}$$

The firing mismatch equation is a real valued function that gives the error in the estimate of the firing angle. If θ_i is the only unknown variable in this equation, then solving by the Newton–Raphson technique yields a solution in about four iterations that is accurate to 10^{-6} radians. The partial derivatives are easily obtained, and for the single variable case

$$\frac{\partial F_{\theta_i}}{\partial \theta_i} = \text{Im}\left\{-j + \sum_{k=1}^{n_h} jk\alpha_k e^{jk\theta_i}\right\} \tag{11}$$

This analysis gives the variation in firing instant as a result of DC ripple. It is assumed that equally spaced timing pulses are generated by an oscillator, phase-locked to the fundamental component of the terminal voltage at the convertor transformer primary winding. Another parameter in the firing mismatch equation is the constant component of the alpha order α_0. This is obtained from the DC-current mismatch

$$I_{d_0} - V_{d_0} Y_{d_0} = 0 \tag{12}$$

where V_{d0}, the DC voltage, is a function of the AC terminal voltage, the DC current, and the convertor switching angles. The DC-current mismatch equations are developed in Section 2.6.

2.3 Voltage and current samples

The six-pulse convertor passes through twelve states per cycle. Six of these are commutation states, and six are 'normal' conducting states. During normal conduction, the positive and negative rails of the DC side are directly connected to different phases of the AC terminal via the commutating reactance in each phase. The kth harmonic component of the DC voltage is therefore

$$V_{dpk} = V_+ - V_- - j\omega k(L_+ + L_-)I_{dk} \tag{13}$$

During a commutation on the positive rail, analysis of Fig. 1 yields

$$V_{dpk} = \frac{L_e V_b + L_b(V_e - jk\omega L_e I_{dk})}{L_e + L_b} - V_0 - jk\omega L_0 I_{dk} \tag{14}$$

and for a commutation on the negative rail

$$V_{dpk} = V_0 - jk\omega L_0 I_{dk} - \frac{L_e V_b + L_b(V_e + jk\omega L_e I_{dk})}{L_e + L_b} \tag{15}$$

From the known conduction pattern in each of the twelve states, eqns. 13, 14 and 15 are used to assemble the twelve samples of the DC voltage. These samples are summarised in Table 1.

Table 1: Construction of DC voltage and AC phase current samples

Sample (p)	Phase-currents			DC voltage (V_{dp})					
	A	B	C	e	b	o	+	−	eqn.
1	I_{c1}	$-I_d$	$I_d - I_{c1}$	A	C	B	.	.	14
2	I_d	$-I_d$	0	.	.	.	A	B	13
3	I_d	$-I_{c2} - I_d$	I_{c2}	C	B	A	.	.	15
4	I_d	0	$-I_d$	.	.	.	A	C	13
5	$I_d - I_{c3}$	I_{c3}	$-I_d$	B	A	C	.	.	14
6	0	I_d	$-I_d$	.	.	.	B	C	13
7	I_{c4}	I_d	$-I_{c4} - I_d$	A	C	B	.	.	15
8	$-I_d$	I_d	0	.	.	.	B	A	13
9	$-I_d$	$I_d - I_{c5}$	I_{c5}	C	B	A	.	.	14
10	$-I_d$	0	I_d	.	.	.	C	A	13
11	$-I_{c6} - I_d$	I_{c6}	I_d	B	A	C	.	.	15
12	0	$-I_d$	I_d	.	.	.	C	B	13

The phase current samples are assembled in a similar manner using the calculated commutation currents and the DC current.

2.4 Sampling functions

In the time domain, the contribution of each voltage sample to the DC voltage is obtained by multiplying by a square pulse periodic function (Fig. 4). The period of the sampling function is the same as the fundamental. Thus in the harmonic domain, the contribution of each voltage sample to the DC voltage harmonics is obtained by convolving its Fourier series with the sampling function Fourier series. The Fourier series for the sampling function in Fig. 4 is

$$\Psi_{pk} = \frac{1}{k\pi}[\cos(ka_p) - \cos(kb_p)] + j\frac{1}{k\pi}[\sin(kb_p) - \sin(ka_p)] \tag{16}$$

$$\Psi_{p0} = \begin{cases} j\dfrac{b_p - a_p}{2\pi} & b_p > a_p \\ j\left[1 - \dfrac{a_p - b_p}{2\pi}\right] & \text{otherwise} \end{cases} \tag{17}$$

The twelve sampling functions are calculated between the limits listed in Table 2. Since the end of one state is the beginning of the next, all of the trigonometric evaluations are used in two consecutive sampling functions, thus halving the number of calculations.

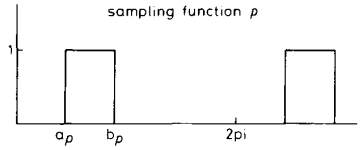

Fig. 4 *Sampling functions used for convolutions*

Table 2: Limits of convertor states for use in sampling functions

Sample (p)	a_p	b_p
1	θ_1	ϕ_1
2	ϕ_1	θ_2
3	θ_2	ϕ_2
4	ϕ_2	θ_3
5	θ_3	ϕ_3
6	ϕ_3	θ_4
7	θ_4	ϕ_4
8	ϕ_4	θ_5
9	θ_5	ϕ_5
10	ϕ_5	θ_6
11	θ_6	ϕ_6
12	ϕ_6	θ_1

2.5 Convolution calculations

Having expressed the DC-voltage samples, phase-current samples, and sampling functions as harmonic phasors, the overall DC voltage and phase currents are obtained by convolution of all the samples with the appropriate sampling functions

$$V_d = \sum_{p=1}^{12} V_{dp} \otimes \Psi_p \tag{18}$$

The convolution of two phasors is given by

$$A_k \otimes B_l = \begin{cases} \frac{1}{2}j(A_k B_l^*)_{(k-l)} - \frac{1}{2}j(A_k B_l)_{(k+l)} & \text{if } k \geq l \\ \frac{1}{2}j(A_k B_l^*)^*_{(l-k)} - \frac{1}{2}j(A_k B_l)_{(k+l)} & \text{otherwise} \end{cases} \tag{19}$$

The conjugate operator makes the convolution non-analytic, and so not differentiable in the complex form. It avoids the need for negative harmonics, however, and it is still possible to obtain all the real partial derivatives which are required for the Newton method. Sum and difference harmonics are generated by the convolution, and since it is required to calculate voltage harmonics up to n_h, the transfer functions must be evaluated up to $2n_h$. Since the convolution operator is linear, the twelve convolutions in eqn. 18 can be decomposed into convolutions of the component phasors

$$V_{dp} \otimes \Psi_p = \sum_{k=1}^{n_h} \sum_{l=0}^{2n_h} V_{dpk} \otimes \Psi_{pl} \tag{20}$$

This equation generates voltage harmonic components of order above n_h which are discarded. By using eqns. 18, 19

and 20, the kth harmonic phasor component of V_d is

$$V_{d_k} = \frac{1}{2} j \sum_{p=1}^{12} \left\{ \sum_{l=k}^{n_h} (V_{dp_l} \Psi^*_{p_{l-k}}) + \sum_{l=1}^{n_h} (V_{dp_l} \Psi^*_{p_{l+k}})^* - \sum_{l=0}^{k} (V_{dp_l} \Psi_{p_{k-l}}) \right\} \quad k > 0 \tag{21}$$

$$V_{d_0} = \frac{1}{2} j \sum_{p=1}^{12} \left\{ \sum_{l=0}^{n_h} (V_{dp_l} \Psi^*_{p_l}) - (V_{dp_0} \Psi_{p_0}) \right\} \tag{22}$$

The derivation of the DC voltage required the convolution of twelve different DC-voltage samples, so by using the same sampling functions, 36 convolutions would be required to obtain the three phase currents. However, referring to Table 1, and using the linearity of the convolution, the phase-A current can be written as

$$I_a = I_d \otimes \{\Psi_2 + \Psi_3 + \Psi_4 + \Psi_5 - \Psi_8 - \Psi_9 - \Psi_{10} - \Psi_{11}\} + I_{c_1} \otimes \Psi_1 - I_{c_3} \otimes \Psi_5 - I_{c_4} \otimes \Psi_7 + I_{c_6} \otimes \Psi_{11} \tag{23}$$

and similarly for the other two phases. This leads to a total of 9 convolutions to calculate the three phase currents.

2.6 Current mismatch equations

The twelve mismatch equations derived so far (i.e. eqns. 6 and 10), relate to the firing angles for the Graetz bridge. All of these equations are functions of the DC-current harmonics. In solving the combined convertor and DC system, it is therefore necessary to include the DC-current harmonics in the overall Jacobian. The corresponding mismatch equations are easily obtained by impressing the calculated DC voltage upon the DC-system representation. The resulting harmonic currents should equal the DC-current harmonics used in the calculation. For the DC system consisting merely of a shunt admittance, the following mismatch equation results:

$$F_{I_k} = V_{d_k} Y_{d_k} - I_{d_k} = 0 \tag{24}$$

For the $k = 0$ equation, I_{dc_0} is the current order, and so is not a variable. This equation is used instead to find the average alpha order in Section 5. The n_h current mismatch equations are complex valued, but not differentiable in the complex form. However, the partial derivatives of the real and imaginary parts can still be obtained.

3 Model verification-independent DC current

By specifying in advance the DC current, and AC terminal voltage (including harmonics), it is possible to solve the convertor state without having to form a Jacobian matrix (or even use an overall iterative process). This is because the twelve convertor mismatch equations become functions of only a single unknown variable. The mismatch equations are therefore solved sequentially using the single variable Newton–Raphson procedure.

In order to compare the equations derived so far with the results of a completely different method, the simple system of Fig. 5 was simulated in the time domain using the program EMTDC. It was found necessary to use a time step of 20 μs, and to simulate 0.5 s to allow transients to decay. Having run the program to the steady state, the DC current was measured, an FFT was performed on the DC current over one fundamental cycle, and the resulting spectrum was used as input to the harmonic domain model. The average alpha order was obtained by taking the constant term of the alpha order spectrum. The parameters for the circuit of Fig. 5 and the controller of Fig. 2 are listed in Table 3. The controller and voltage source were chosen so as to cause large uncharacteristic harmonics.

Table 3: Parameters for test convertor. The voltage source is distorted by 0.1 p.u. positive sequence 2nd and 0.1 pu negative sequence 3rd harmonic

X_{ca}, X_{cb}, X_{cc}	0.1786 p.u.
X_d	3.3 p.u. = 0.05H
R_d	0.0087 p.u. = 0.041 Ω
V_t	24 kV ll (+ve seq.)
S_{base}	122 MVA
G	0.27778 rad/p.u.
T	0.005 s
P	1.5
I	0.005 s
PLO	perfect

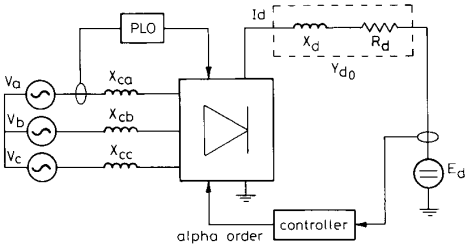

Fig. 5 *Six-pulse convertor circuit*

Having read in the above data, the harmonic domain program iteratively calculates the six firing instants using

$$\theta_{i_{(N+1)}} = \theta_{i_{(N)}} - \frac{F_{\theta_i}}{(\partial F_{\theta_i})/\partial \theta_i} \tag{25}$$

Next, the end of commutation angles are calculated by the same Newton–Raphson method applied to the commutation mismatch. With the convertor state now known, the sampling functions are calculated and convolved with the DC-voltage samples to give the DC voltage. Finally, the DC and commutation currents are used to find the phase currents, using the same sampling functions.

The time-domain solution serves to verify the harmonic analysis, if upon comparison a close agreement is found in the calculated DC voltage and phase currents. These comparisons are made in Figs. 6 to 9, which also give a graphical indication of the solution by sampling and convolution. The comparison of the DC-voltage spectra in Fig. 8, shows that, despite using truncated Fourier series for the sampling functions and DC current, the calculated results agree to the 50th harmonic. Such a close agreement between two such different methods of solution serves to verify both of them. In addition, the convertor model developed by Wood has been verified against EMTDC for low-order harmonics, giving a close agreement between all three models for those harmonics. We can therefore conclude that the process of harmonic transfer across the convertor has been accurately solved by the use of convolved sampling functions.

One advantage of the harmonic domain is that it is possible to include only significant harmonics in the analysis. The mode was run using only harmonics 1, 2 and 3 for the AC voltage (since this is what the source is defined to be), and harmonics 0, 1, 2 and 6 for the DC current. The resulting DC-voltage spectra are compared

in Fig. 10. The close match indicates the feasibility of solving the full system (with dependent DC current and terminal voltage) in two stages. In the first stage, only significant harmonics are considered, in order to get very close to the solution quickly. In the second stage, when all harmonics are included in the Jacobian, the starting point may be so good that it is not necessary to invert the Jacobian matrix at each iteration.

It should be noted that the system compared here is unrealistically 'bad' in order to show up any deficiencies in the model.

4 Dependent DC current

In this Section, a hybrid Gauss–Seidel and Newton solution to the convertor is developed for the case in which the DC current is unknown. An iterative solution technique is required, as there are 113 nonlinear equations in as many unknowns to be solved (for 50 harmonics). The unknowns are the real and imaginary parts of the DC-ripple harmonics, the convertor switching angles, and the average alpha order.

Assuming the DC current to be ripple free, and approximating the average alpha order α_0 from

$$V_{d_0} = \frac{3\sqrt{(2)}}{\pi} V_t \cos \alpha_0 - \frac{3}{\pi} X_c I_{d_0} \tag{26}$$

the independent DC-current solution of the previous section is applied to obtain an estimate of the DC voltage. This voltage is impressed on the DC-system model to obtain an estimate of the DC current. Using the DC-current estimate, the DC voltage is updated and used to obtain a better estimate of the DC current. This estimate of the DC current is the starting point for the iterative process. It is typically accurate to within 3% for the ripple harmonics, but only 50% for the DC term.

The inaccuracy in the DC term arises from the impossibility of calculating α_0 accurately (in analytic form). The DC-current term critically depends on the DC-voltage term, which is a strong function of α_0, and to a lesser extent on the firing and overlap angle variation, AC-voltage distortion, DC ripple and commutation reactance mismatch. The calculation of α_0 must therefore be part of the iterative solution. Small variations in α_0 were found not to affect the DC ripple very much, but yet to have a large effect on the DC current. The convertor solution is therefore partitioned into two sub-problems, which are independent of each other (for small variations in α_0); calculation of that value of α_0 which gives the required DC current, and calculation of the DC-current ripple. Calculation of the DC ripple is obtained efficiently by means of the Gauss–Seidel method, whereas α_0 is found by linearising at each Gauss–Seidel step the dependence of the I_{d_0} mismatch to α_0. This linearisation is very

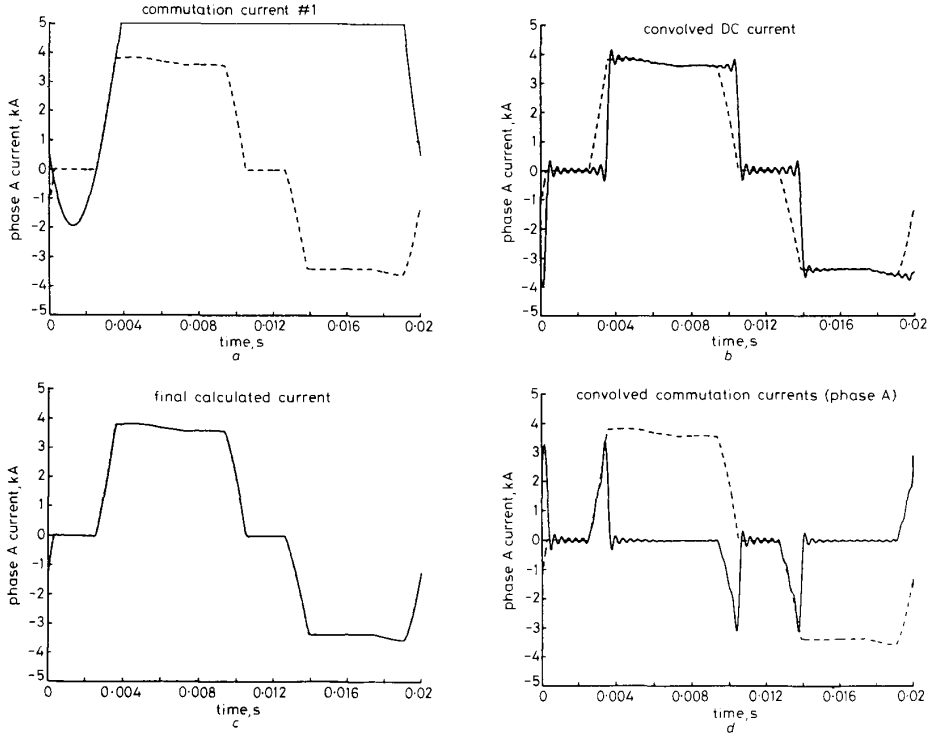

Fig. 6 *Construction of phase-A current*

- - - - EMTDC ——— calculated

a The periodic sample of the first commutation current

b The DC current convolved with its sampling function

c The four convolved commutation currents

d The sum of the convolved commutation and DC currents

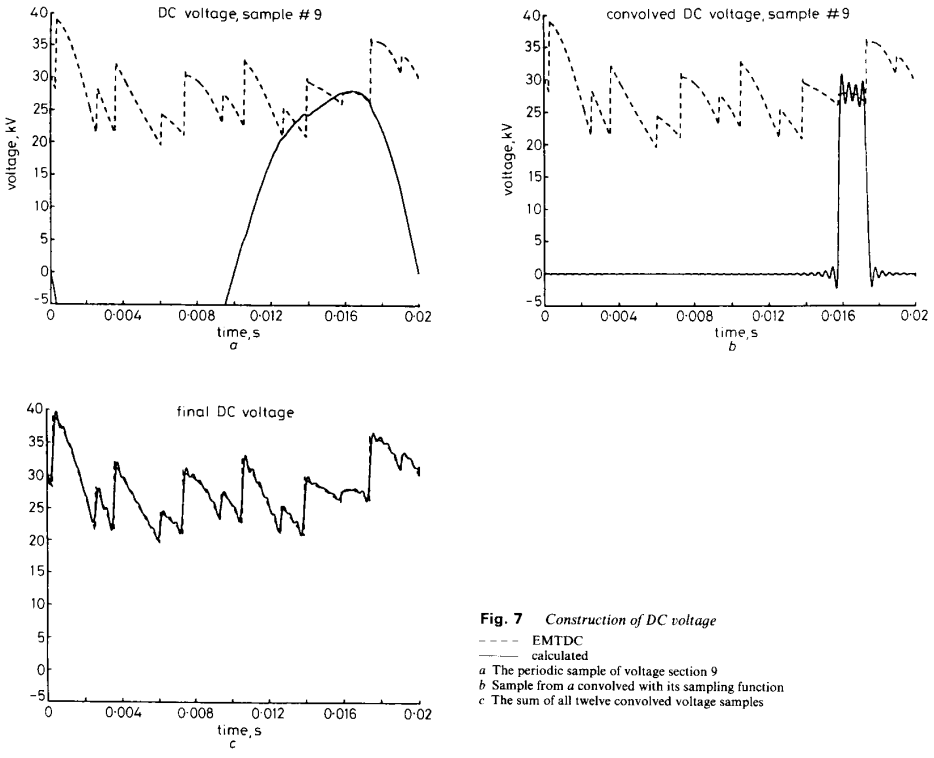

Fig. 7 *Construction of DC voltage*
- - - - EMTDC
——— calculated
a The periodic sample of voltage section 9
b Sample from *a* convolved with its sampling function
c The sum of all twelve convolved voltage samples

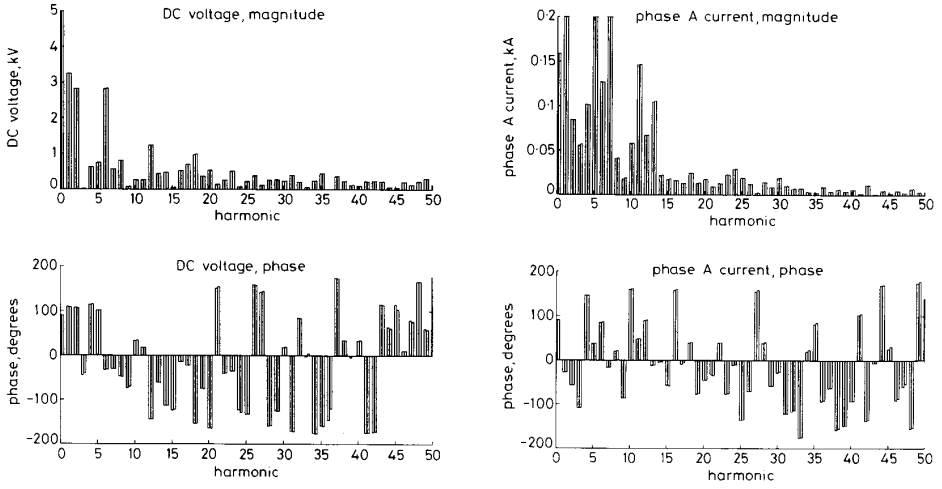

Fig. 8 *Comparison of spectra for DC voltage of test convertor*
left = calculated right = EMTDC

Fig. 9 *Comparison of spectra for phase-A current of test convertor*
left = calculated right = EMTDC

similar to the single variable Newton–Raphson method, except that at each step the function to be solved is modified slightly by the parallel Gauss–Seidel step. The linear-

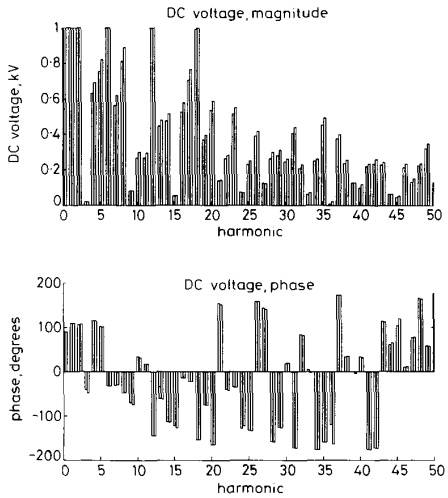

Fig. 10 *Effect of considering only DC-current harmonics 0, 1, 2 and 6*
left = full right = reduced

isation requires the partial derivative

$$\frac{\partial(\mathrm{Im}\{V_{d_0}Y_{d_0}\}-I_{d_0})}{\partial\alpha_0} = \frac{1}{2}jY_{d_0}\left[\sum_{i=1}^{6}\frac{\partial\,\mathrm{Im}\{V_{d_0}\}}{\partial\theta_i}\frac{\partial\theta_i}{\partial\alpha_0}+\sum_{i=1}^{6}\frac{\partial\,\mathrm{Im}\{V_{d_0}\}}{\partial\phi_i}\frac{\partial\phi_i}{\partial\theta_i}\frac{\partial\theta_i}{\partial\alpha_0}\right] \quad (27)$$

where

$$\frac{\partial\,\mathrm{Im}\{V_{d_0}\}}{\partial\phi_i} = \mathrm{Im}\left\{\left(V_{d(2i-1)0}\frac{\partial\Psi_{2i0}}{\partial\phi_i}-\sum_{l=0}^{n_h}V_{d(2i-1)l}\left(\frac{\partial\Psi_{2il}}{\partial\phi_i}\right)^*\right.\right. \left.\left.-V_{d(2i)0}\frac{\partial\Psi_{2i0}}{\partial\phi_i}+\sum_{l=0}^{n_h}V_{d(2i)l}\left(\frac{\partial\Psi_{2il}}{\partial\phi_i}\right)^*\right)\right\} \quad (28)$$

$$\frac{\partial\,\mathrm{Im}\{V_{d_0}\}}{\partial\theta_i} = \mathrm{Im}\left\{\left(V_{d(2i-1)0}\frac{\partial\Psi_{(2i-1)0}}{\partial\phi_i}\right.\right. -\sum_{l=0}^{n_h}V_{d(2i-2)l}\left(\frac{\partial\Psi_{(2i-1)l}}{\partial\phi_i}\right)^*-V_{d(2i-1)0}\frac{\partial\Psi_{(2i-1)0}}{\partial\phi_i} \left.\left.+\sum_{l=0}^{n_h}V_{d(2i-1)l}\left(\frac{\partial\Psi_{(2i-1)l}}{\partial\phi_i}\right)^*\right)\right\} \quad (29)$$

$$\frac{\partial\theta_i}{\partial\alpha_0} = \frac{-1}{\mathrm{Im}\{-j+\sum_{k=1}^{n_h}(jk\alpha_{i_k}e^{jk\theta_i})\}} \quad (30)$$

$$\frac{\partial\phi_i}{\partial\theta_i} = \frac{-\,\mathrm{Im}\{\sum_{k=1}^{n_h}jkI_{c_k}e^{jk\theta_i}\}}{\mathrm{Im}\{\sum_{k=1}^{n_h}jkF_{\phi ik}e^{jk\phi_i}\}} \quad (31)$$

At each iteration α_0 is updated using

$$\alpha_0^{N+1} = \alpha_0^N - \frac{\mathrm{Im}\{V_{d_0}Y_{d_0}\}-I_{d_0}}{[\partial(\mathrm{Im}\{V_{d_0}Y_{d_0}\}-I_{d_0})]/\partial\alpha_0} \quad (32)$$

while the DC ripple is updated using the methods described in Section 2.

Convergence is deemed to have occurred when for every harmonic of DC current

$$\frac{|F_{I_k}|}{|I_{d_k}|} < 0.0005 \quad |I_{d_k}| > 0.0001 \text{ p.u.} \quad (33)$$

That is, the relative mismatch (rather than the absolute mismatch) is less than a predetermined tolerance. For the test case of the previous Section, five iterations are required to obtain this accuracy. Convergence is initially very fast, typical of the Newton–Raphson solution, whereas in the proximity of the solution, convergence is more influenced by the Gauss–Seidel solution. This is because, once the Newton–Raphson part of the solution has obtained a moderately accurate α_0, further small changes to α_0 do not affect the Gauss–Seidel solution of the DC-current ripple. The overall solution is so fast and strong with this method, that it is not appropriate to develop a full Newton-type solution employing a Jacobian (unless the terminal voltage is not infinitely sourced). Table 4 shows the progress of the solution for the DC term and 6th harmonic on the DC side.

Table 4: Convergence of DC-current relative error

Harmonic	Relative error for ith iteration				
i	1	2	3	4	5
DC	0.328	0.0176	0.0044	0.000323	0.000234
6th	0.0846	0.0114	0.000778	0.000179	0.000014

5 Partial-convertor models

In this Section, parts of the developed model are disabled in order to determine their relative influence on the overall model. This also enables a comparison to be made between the complete solution developed here, and the results that might be expected from some of the other convertor models mentioned in the Introduction. The convertor to be investigated is again that of Fig. 5, but with the circuit parameters adjusted, as in Table 5, to match as closely as possible the CIGRE benchmark model [9].

Table 5: Parameters for cut down version of CIGRE benchmark model

X_{ca}, X_{cb}, X_{cc}	0.18 p.u.
X_d	0.994666 H
R_d	5 Ω
V_t	213.4557 kV II (+ve seq.)
S_{base}	603.73 MVA
G	0.5
T	0.001 s
P	1.0989
I	0.0091 s
PLO	perfect

The method used is to disable part of the model so that a particular effect is not represented. The system is then solved with a harmonic source applied directly to the disabled feature of the model. The system is then solved again with the full convertor model. For example, if the effect of DC ripple on commutation duration, and hence DC voltage, is to be determined, a harmonic

current source is placed on the DC side. The convertor is then solved both with and without this effect included in the calculation of the commutation duration. This methodology allows the contribution of different aspects of the model to the overall solution to be determined.

5.1 Commutation duration

The effect of DC-current ripple on the commutation is limited to two main effects that have been solved accurately. The DC ripple contributes to the commutation current, thus changing the shape of the commutation. This effect is expected to be small, since the DC ripple is small compared with the line to line voltage shorted through the commutating reactance. The other effect relates to the fact that the ripple superimposed on the DC current affects the duration of the commutation directly (since the commutation ends when $I_c = I_d$). These two effects are disabled independently in this Section.

With 5% of the second harmonic current injected on the DC side, the DC voltage was calculated accurately to serve as a reference. Next, the program was modified so that, although the commutation current was still a function of the DC ripple, the commutation was defined to end when the commutating current was equal to the constant component of the DC current (rather than the instantaneous value). The DC-voltage spectra for the two cases are compared in Fig. 11.

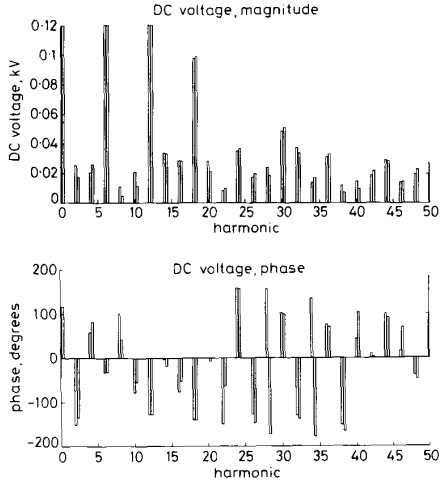

Fig. 11 *Effect of intercepting commutation with constant DC-current component rather than instantaneous value (on DC voltage)*
left = ripple, right = no ripple

For the second test, the commutation current itself was made independent of the DC-current ripple. The end of commutation, however, was restored to the original definition of occurring when the commutation current is equal to the instantaneous value of the DC current. This situation corresponds to the later model of Yacamini [3], which included the effect of firing-angle variation. The DC-voltage spectra are compared in Fig. 12. From the Figures, it can be seen that there is a general close agreement, but that in both cases the greatest difference is in the phase of the non-characteristic harmonics. For levels of DC ripple greater than 5%, it appears necessary to include all aspects of the DC ripple in the commutation calculation, in order to obtain accurate results for the non-characteristic harmonics. However, it is far more important to include the effect of DC ripple in calculating the commutation duration, than in calculating the commutation current itself. In any case, with the model developed here, it is easy and natural to model all aspects of the commutation.

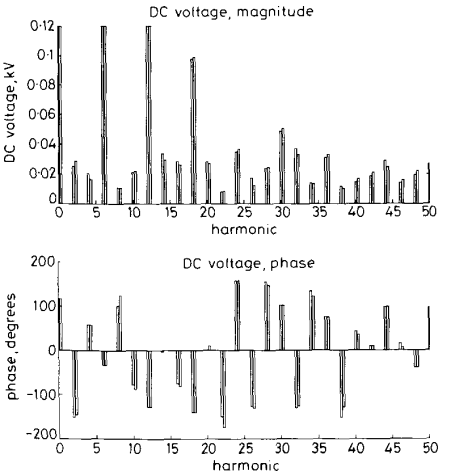

Fig. 12 *Effect of neglecting DC-ripple current component of commutation current*
left = exact, right = approximate

5.2 Firing instant calculation

DC ripple is picked up by the convertor controller and leads to firing-angle variation. By locking the alpha order to the average value, any variation in firing angle is prevented. This enables the effect of firing-angle variation to be determined. The DC ripple was again set at 5% of the second harmonic. The results are presented in Fig. 13 for the case of DC-voltage spectra.

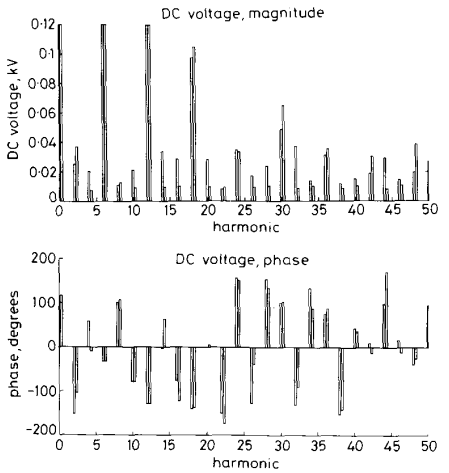

Fig. 13 *Effect of neglecting firing angle variation on DC voltage determined by locking the alpha order to a constant value*
left = not locked, right = locked

Overall, these results show that firing imbalance must be modelled accurately. If the DC ripple is expected to be large, ignoring any aspect of the DC ripple in the commutation analysis can lead to errors of the order of 10% in the DC-harmonic voltage magnitudes. These results are similar to those that could be expected from a model that assumed a ripple-free DC current in the calculation of the DC voltage. If the DC current is a direct function of the DC voltage, then these errors will carry through to the phase currents. Even larger errors occur in the DC-voltage harmonic phase angles. We conclude that it is necessary to include all aspects of the DC ripple in the communication analysis if the DC ripple is substantial, and the DC-ripple harmonics are dependent variables.

6 Conclusion

A set of steady-state equations has been developed that describe the convertor in the harmonic domain. By convolving sampled quantities sampling functions, all the relevant convertor interactions have been modelled using complex phasors. The convolution method leads to simple but accurate mismatch equations, for which all the partial derivatives have been obtained.

By keeping the DC current and AC terminal voltage independent, it is possible to avoid solving a system of nonlinear equations for the convertor. This technique has been applied to a six-pulse convertor, and the equations verified against a time-domain solution.

A solution for the convertor has been found for the case in which the DC-current harmonics are dependent variables. This was achieved by linearising the dependence of the DC current on the average alpha order at each iteration of the Gauss–Seidel solution. Convergence was found to be rapid, even for a highly distorted terminal voltage.

Using a simplified version of the CIGRE benchmark model, the effect of DC-ripple current on the commutation and firing-pulse processes has been determined, and found to be significant when the DC ripple is large, especially for the noncharacteristic harmonics of the DC voltage.

The mismatch equations developed here are suitable for integration into an overall harmonic domain solution of a convertor embedded in a combined AC and DC system. Further work is directed towards extending the model to twelve pulses, including more elaborate control functions, and modelling the convertor transformer.

7 References

1 YACAMINI, R., and DE OLIVEIRA, J.C.: 'Harmonics in multiple convertor systems: a generalised approach', *IEE Proc. B*, 1980, **127**, (2), pp. 96–106

2 WOOD, A.R.: 'An analysis of non-ideal HVDC convertor behaviour in the frequency domain, and a new control proposal'. PhD Thesis, University of Canterbury, New Zealand, 1993

3 YACAMINI, R., and DE OLIVEIRA, J.C.: 'Comprehensive calculation of convertor harmonics with system impedances and control representation', *IEE Proc. B*, 1986, **133**, (2), pp. 95–102

4 EGGLESTON, J.F.: 'Harmonic modelling of transmission systems containing synchronous machines and static convertors'. PhD Thesis, University of Canterbury, New Zealand, 1985

5 CALLAGHAN, C.D.: 'Three phase integrated load and harmonic flows'. PhD Thesis, University of Canterbury, New Zealand, 1985

6 CARBONE, R., FANTAUZZI, M., GAGLIARDI, F., and TESTA, A.: 'Some considerations on the iterative harmonic analysis convergence'. ICHPS V, 1992, pp. 49–55

7 VALCÁRCEL, M.: 'Análisis del régimen permanente de los sistemas eléctricos de potencia con elementos no lineales mediante un método de reparto de cargas con armónicos'. Tesis Doctoral, Universidad Poliecnica de Madrid, 1991

8 FERREIRA DE JESUS, J.M.D.: 'D.C. transmission system harmonic analysis and stability using describing functions'. PhD Thesis, University of London, 1982

9 SZECHTMAN, M., WEISS, T., and THIO, C.V.: 'First benchmark model for HVdc control studies', *Electra*, 1991, **135**, pp. 55–75